STABILITATEA MASELOR FOSFATICE FLUORURATE PE ALIAJE DE CoCrMo
ABOUT STABILITY OF ELECTRODEPOSITED FLUORIDATED PHOSPHATE MASSES ON CoCrMo ALLOYS

DANIELA COVACIU ROMONȚI, GEORGETA VOICU∗, DANIELA IONIȚĂ, IOANA DEMETRESCU
Universitatea POLITEHNICA București, str. G. Polizu, nr. 1, 011061, sect. 1, București, Romania

CoCrMo alloys are extensively used in tissue engineering in both dental and orthopaedic applications and are highly recommended due to the good ratio quality /price comparing with other metallic biomaterials. The present approach is related to electrodeposition of fluoridated phosphate masses with good ratio calcium to phosphorus close to the one existing in bone.

SEM and EDX analysis confirm that the electrochemical method for deposition of fluoridated apatite on CoCrMo is efficient and the results were quantified using electrochemical and mechanical measurements.

Aliajele de CoCrMo sunt des utilizate în ingineria tisulară, atât în aplicațiile stomatologice cât și în cele ortopedice și sunt recomandate datorită raportului bun calitate/ preț comparându-le cu alte biomateriale metalice. Abordarea actuală este legată de electrodepunerea maselor fosfatice fluorurate cu raport bun calciu fosfor, apropiat de raportul molar existent în os.

Analizele SEM și EDX confirmă că metoda electrochimică pentru depunerea maselor apatitice pe aliajul de CoCrMo este eficientă iar rezutatele au fost cuantificate prin măsurători electrochimice și mecanice.

1. Introduction

Having very good mechanical properties as castability, corrosion and wear resistance CoCrMo alloys [1] noowdays, are extensively used in tissue engineering in both dental and orthopaedic applications [2,3]. Even as heads in artificial joints. CoCrMo alloys have been introduced in bioapplications at the begging of the last century, but due especially to its problems with ion release for a period of time was used with limitations. A remarkable comeback was known in its using after introducing largely the surface engineering procedures [4,5] and the type of Ni-free alloy according to ASTM F-75 standard [6]. In medicine regeneration, CoCrMo alloys are highly recommended due to the good ratio quality /price and comparing with other metallic biomaterials as stainless steels [7] which have disadvantage in corrosion resistance or with titanium alloys which have demerit in wear resistance [2], despite the large variety of surface modifications proposed for enhancing their performance especially at the surface level [8].

The wear resistance of the CoCrMo alloys is due to the carbide structure found in both cast and wrought alloys. The hardness and elongation is attributable to the ε martensite transformation induced by strain [9]. The resistance to corrosion is

due to its passive film formed at the surface in various bioliquids [10]. The existence of a small amount of nickel as an impurity, despite the fact International Agency for Research on Cancer (IARC) of the World Health Organization (WHO) estimates that nickel is carcinogenic [11], is able to maintain workability. More recently, taking into account the bacteria extension, and knowing the silver effect in enhancing antibacterial function new coatings having antibacterial inhibition effect were elaborated on the CoCrMo alloy surface [12] including hydroxyapatite (HA) as bioactive component and silver as antibacterian agent as well. Hydroxyapatite as bioactive coating was elaborated via various procedures [13,14] leading to various properties. It has been reported that plasma-sprayed HA coatings dissolve and degrade quickly, resulting in the weakening of the coating-substrate bonding or the implant fixation to the host tissues [15]. For this reason any changes to the HA that result in a higher chemical stability would be an advantage.

Impregnations to the HA crystal structure the chemical elements such as Fluoride by substituting OH^- groups was performed successfully on various alloys [16,17].

The present approach is related to electrodeposition of fluoridated phosphate masses with good ratio calcium to phosphorus close to the

─────────────
∗ Autor corespondent/*Corresponding author*,
E-mail: getav2001@yahoo.co.uk

one existing in bone, in order to provide resistance to dissolution. Firstly the aim of present research is trying to establish a relation between electrochemical behaviour of such coating from corrosion parameters in bioliquids and from ions release evaluation with mechanical properties. A comparison of electrochemical stability of the coated alloy in saliva and in physiological NaCl solution is discussed as well.

2. Experimental

For electrodeposition of phosphate masses were used samples of CoCrMo. Samples were polished on SiC abrasive papers (600, 800 and 1200) and after that etched in HF 4% for 2 minutes. For 15 minutes the samples were ultrasonicated in acetone and ethanol in order to remove particles from the SiC paper. Finally the samples were rinsed in distilled water and dried at the room temperature. The content of electrolyte solution was $(NH_4)_2HPO_4$ 0.025 M, NH_4F 0.012 M and $CaCl_2·2H_2O$ 0.042 M, almost similar with the electrolyte used in literature for electrodeposition of fluoridated hydroxyapatite on stainless steel titanium [18]. A volume of H_2O_2 3% was added in order to enhance the deposition process of dense coating by the release of H_2 gas and production of hydroxyl ions. The chemical composition of CoCrMo alloy it's according to ASTM F75 [6].

2.1. Coating process

The coating process was performed at two different temperatures: 28^oC (sample A) and at 22^oC (sample B) using a electrochemical cell (Figure 1.) with a platinum plate as counter electrode (anode), Ag/AgCl as reference electrode and CoCrMo as working electrode (cathode). Working parameters are presented in Table 1. All the experiments were performed using a PGZ 301 potentiostat/ galvanostat controlled by a computer equipped with Volta Master 4 Software.

After electrodeposition all samples were calcinated at 400^0C temperature for 1 hour. Thermal treatment was made in order to increase the crystallinity and the purity of the coated CoCrMo samples. Calcination was also, beneficial for strengthening the bonds of apatite coatings. Figure 2 shows variation of potential in time of electrochemical deposition of fluoridated apatite coatings on CoCrMo samples.
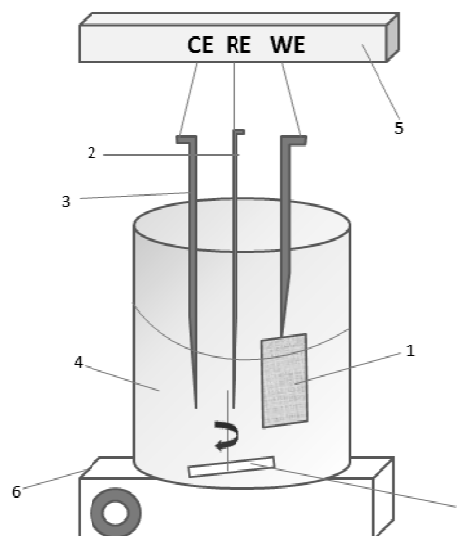
Fig. 1 - Electrolytic cell scheme used in coating process: 1-WE (CoCrMo), 2-RE (Ag/AgCl), 3-CE (Pt), 4-electrolyte, 5-potentiostat/ galvanostat, 6-magnetic stirrer, 7-stirrer/ *Schema celulei electrochimice folosite în procesul de depunere: 1-EL (CoCrMo), 2-ER (Ag/AgCl), 3-CE (Pt), 4-soluție electrolit, 5-potențiostat/ galvanostat, 6-agitator magnetic, 7-agitator.*
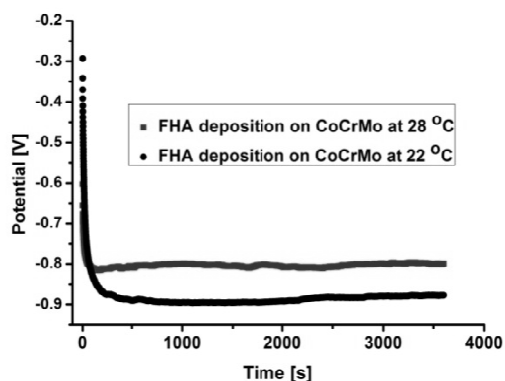
Fig. 2 - Coating process/ *Procesul de depunere.*

Curve equations for coating process are shown below; equation (1) for coated CoCrMo at 28^oC have standard deviation, $R^2 = 0.65$ and the second equation (2) for coated CoCrMo at 22^oC have standard deviation, $R^2 = 0.92$

$$y = -0.80368 + 0.1388 \cdot e^{0.07442x} \qquad (1)$$
$$y = -0.88625 + 0.43206 \cdot e^{-0.02516x} \qquad (2)$$

The mechanism of electrolytic deposition can be described as a series of electrochemical reactions.

Table 1

Working parameters for coating process/ *Parametri de lucru pentru procesul de depunere*

CoCrMo Sample *Proba CoCrMo*	Current Density *Densitate de curent* [mA/cm^2]	Electrodeposition time / *Timp de electrodepunere* [min]	Deposition temperature *Temperatura de depunere* [^oC]
A	-1	60	28
B			22

The possible sources of OH⁻ at the cathode are [19]

$$O_2 + 2H_2O + 4e^- \rightarrow 4HO^- \qquad (3)$$
$$NO_3^- + H_2O + 2e^- \rightarrow 2HO^- + NO_2 \qquad (4)$$
$$2H_2O + 2e^- \rightarrow H_2 + 2HO^- \qquad (5)$$
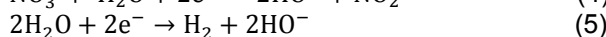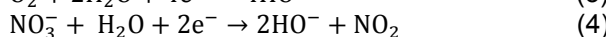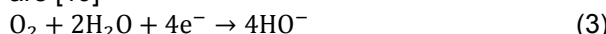
Hydroxide ions, generated during the electrodeposition process, resulted in an increase of the pH in the vicinity of the cathode; which led to the occurrence of the following reactions:

$$H_2PO_4^- + e^- \rightarrow HPO_4^{2-} + \tfrac{1}{2}H_2 \qquad (6)$$
$$H_2PO_4^- + 2e^- \rightarrow PO_4^{3-} + H_2 \qquad (7)$$
$$H_2PO_4^- \rightarrow HPO_4^{2-} + H^+ \qquad (8)$$
$$HPO_4^{2-} \rightarrow PO_4^{3-} + H^+ \qquad (9)$$
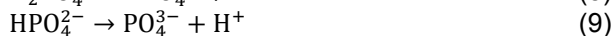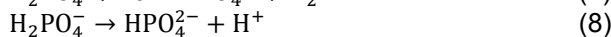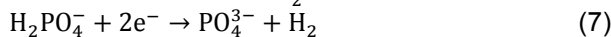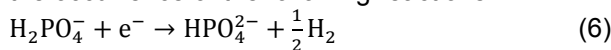
The precipitation of phosphate ions occurred due to the acid-base reactions, which are vital for the crystallization process of formation of FHA coating film according to the following reaction:

$$H_2PO_4^- + HO^- \rightarrow HPO_4^{2-} + H_2O \qquad (10)$$
$$H_2PO_4^- + H_2O + 2e^- \rightarrow$$
$$H_2PO_3^- + 2HO^- \qquad (11)$$
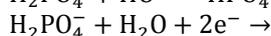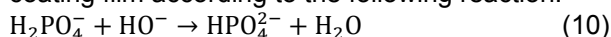
The suitable local chemical environment in the vicinity of the cathode enabled the HPO_4^{2-} ions to react with the Ca^{2+} ions [17].

$$Ca^{2+} + HPO_4^{2-} + H_2O \rightarrow$$
$$CaHPO_4 \cdot 2H_2O \qquad (12)$$
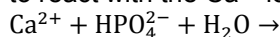
The coating, after alkaline treatment, was converted to HA according to the following reaction:

$$10CaHPO_4 + 2HO^- \rightarrow$$
$$Ca_{10}(PO_4)_6(OH)_2 +$$
$$4PO_4^{3-} 10H^+ \qquad (13)$$
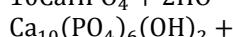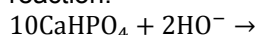
Calcium deficient hydroxyapatite was formed as follows [20]

$$(10 - x)Ca^{2+} + (6 - x)PO_4^{3-} +$$
$$xHPO_4^- + (2 - x)HO^- \rightarrow$$
$$Ca_{10-x}(HPO_4)_x(PO_4)_{6-x}(OH)_{2-x} \qquad (14)$$
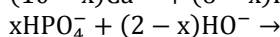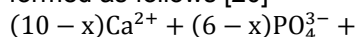
where $0 < x \leq 2$.

Addition of NaF into the electrolyte led to the occurrence of the following reactions. At the early stage, Ca^{2+} ions rapidly consumed the F^- ions in the electrolyte to form CaF_2 which can be expressed as follows [20]

$$Ca_5(PO_4)_3OH + 10F^- +$$
$$(7 - n)H^+ \rightarrow$$
$$5CaF_2 + H_2O +$$
$$(3 - n)H_2PO_4^- + nH_2PO_4^{2-} \qquad (15)$$
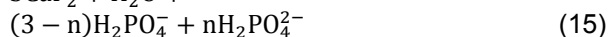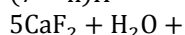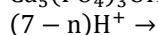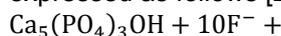
CaF_2 particles reacted with the HPO_4^{2-} ions in the solution to form FHA [20]

$$5CaF_2 + (3 - n)H_2PO_4^- + nHPO_4^{2-}$$
$$+(1 - x)H_2O \rightarrow Ca_5(PO_4)_3(OH)_{1-x}F_x +$$
$$(10 - x)F^- + (7 - x - n)H^+$$

where $(0 < x < 1, 0 < n < 3)$ $\qquad (16)$
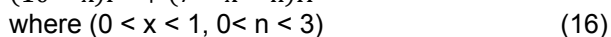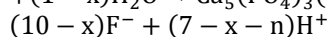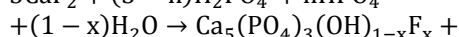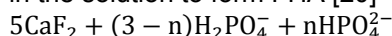
Combining reactions (15) and (16) resulted in the formation of FHA via the following reaction:

$$10Ca^{2+} + 6PO_4^{3-} +$$
$$xF^- + (2 - x)HO^- \rightarrow$$
$$Ca_{10}(PO_4)_6F_x(OH)_{2-x} \qquad (17)$$
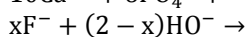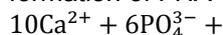
3. Results and discussions

3.1. X-Ray Diffraction Analysis

X-Ray Diffraction analysis was performed for the coated samples of CoCrMo at 22ºC with Empirean PANalytical Diffractometer with radiation Cuα (λ=1.5406Å). The acquisition was done from 10 to 80 degrees 2θ with 0.02 degres step and acquisition time with 2 seconds step. Incidence angle was 1 degree. In Figure 3 is presented XRD analysis for coated CoCrMo samples.

From the XRD analysis it can be observed the deceleration of the mineralogical crystalline phases of fluorohydroxyapatite and $CaHPO_4$.
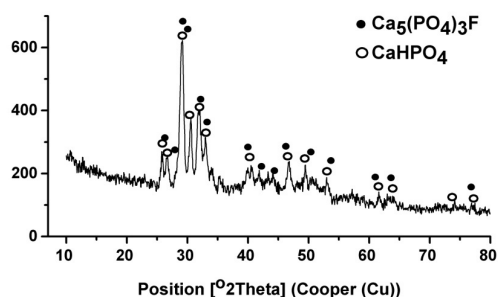
Fig. 3 - XRD analysis of coated CoCrMo/ *Analiza XRD a probelor acoperite de CoCrMo.*

3.2. Scanning electron microscopy analysis

Coated samples of CoCrMo alloy were investigated with a scanning electron microscope HITACHI, S-2600N Model coupled with energy-dispersive X-ray spectroscopy (EDX) for morphology determinations. In Figure 4 are presented images with SEM characterization.

The coated CoCrMo samples shows morphologies which are characteristic to hydroxyapatite according to literature data and the synthesized deposit on CoCrMo alloy consists of spherical particles formed of plaques with very small dimensions (Figure 4). The coating is not uniform on all over the surface probably due to deposition conditions.

The fluoride presence was not observed in elemental analysis, due to the fact that the scanning electron microscope used was limited and does not detect halogens, but the fluoride existence in the coating was confirmed from FT-IR spectra at 719 cm⁻¹. In the literature, Freund, describes a relation between the introduction of fluoride in hydroxyapatite and the increase of a band around 720-740 cm⁻¹ [21].

The difference between coated CoCrMo at 28°C and the coated CoCrMo at 22°C shows a better adherence on the metallic substrate and a more uniform deposition for the electrochemical deposition carried at 22 degrees.
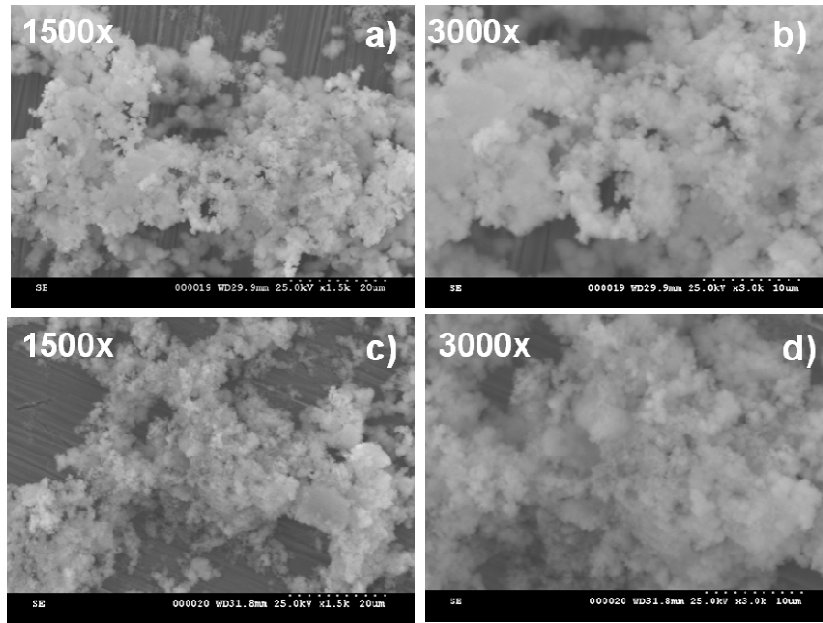
Fig. 4 - SEM images of apatite coatings: a), b) Coated CoCrMo at 28°C; c), d) Coated CoCrMo at 22°C/ *Imagini SEM depuneri apatitice: a), b) CoCrMo acoperit la 28°C, c), d) CoCrMo acoperit la 22°C.*
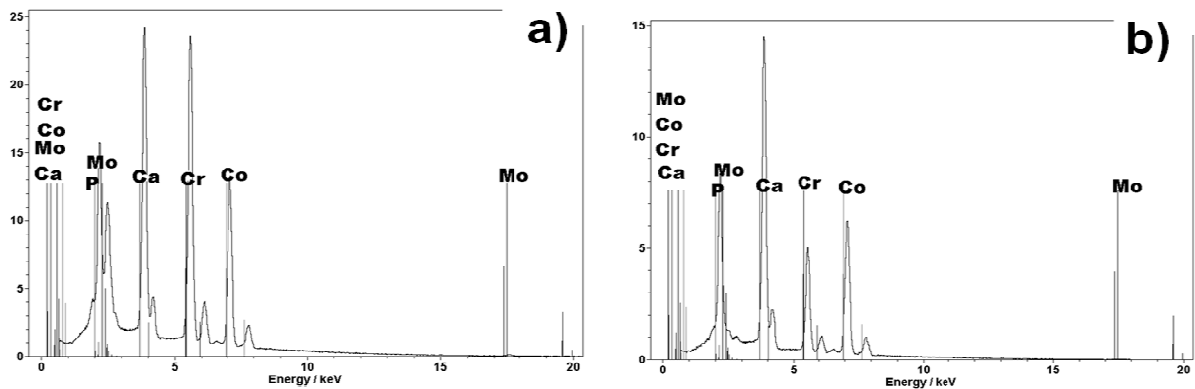
Fig. 5 -EDX spectra of apatite coatings: a) Coated CoCrMo at 28°C; b) Coated CoCrMo at 22°C/ *Spectrul EDX: a) CoCrMo acoperit la 28°C; b) CoCrMo acoperit la 22°C*
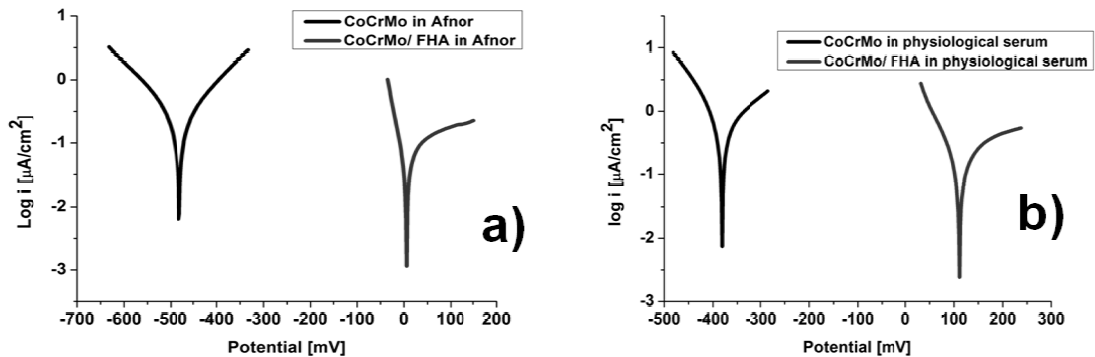
Fig. 6 - Tafel plots for coated and uncoated CoCrMo alloy/ *Curbele Tafel pentru aliajul CoCrMo.*

Figure 5 shows EDX spectra of coated CoCrMo samples and permit la calculation of molar raports Ca/P.

The EDX spectra analysis revealed the presence of calcium and phosphorus, but also the presence of ions substrate, cobalt, chromium and

molybdenum. Molar ratios of phosphate masses of coated CoCrMo alloy are 1.40 for coated CoCrMo at 28°C and 1.88 for coated CoCrMo at 22°C.

EDX analyses shows that CoCrMo sample coating at 28°C is a little bit deficient in calcium, but CoCrMo sample at 22°C is easily overcome in calcium, being much closer to the molar raport Ca/P in bones. Next determinations for characterization of the coated CoCrMo were performed on coated CoCrMo at 22°C.

3.3. Stability of CoCrMo coated with phosphate masses in saline solution and artificial saliva

3.3.1. Electrochemical characterization

Application of fluoridated hydroxyapatite (FHA), $Ca_{10}(PO_4)_6(OH)_{2x}F_x$ where $0 < x < 2$ is the degree of fluoridation (FHA) in comparison with HA coating, could provide better stability as can be seen from electrochemical data and ions relelase determinations.

CoCrMo samples and coated CoCrMo samples were characterized in saline solution (NaCl 0.9% wt %) and in artificial saliva by electrochemical methods, such as Tafel plots, electrochemical impedance spectroscopy and cyclic voltammetry. The chemical composition of artificial saliva Afnor is presented in Table 2.

Tafel plots

The Tafel plots determination were carried in the interval – 200/+ 200mV in reference to open circuit potential and with a scan rate of 2mV/seconds. The determinations were performed using the same three electrodes system as the system used for coating process using artificial saliva and psysiological serum (NaCl 0.9% wt%) as electrolytes.

The polarization curves obtained by VoltaMaster 4 Software are presented in Figure 6.

The smallest current density values (Table 3) were recorded in case of coated CoCrMo alloy immersed in artificial saliva, but in both solutions the coated alloy has a good corrosion resistance.
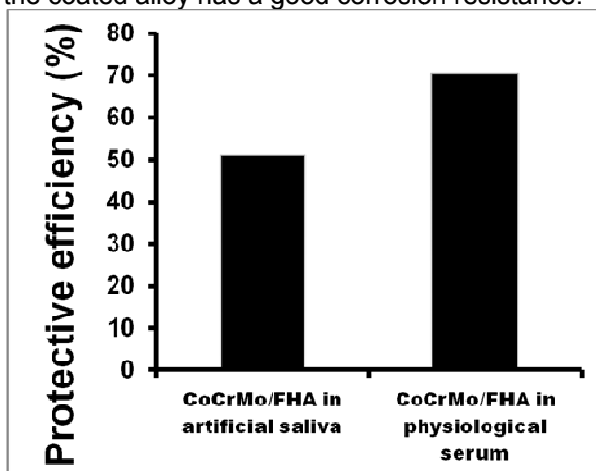
Fig. 7 - Protective efficiency/ *Eficiența acoperirii.*

According to obtained data from Tafel plots it is obvious that corrosion rate is smallest in case of coated alloy and we can confirm that the coverage with fluoridated phosphate masses improve the anticorrosion properties.

The corrosion rates are lower when the alloy is coated and in saline solution are higher than in artificial saliva, the latter being less aggressive. Polarization resistances are enhanced by phosphate masses and corrosion potentials values are displaced from electronegative to electropositive domain, indicating a possible passive character.

As far as the bioactivity is concerned, porosity is a crucial parameter, since it influences the interactions at the implant host tissue interface, especially the reaction rate. A porous coating allows a deeper penetration of cells inside the biomaterial, and thus higher levels of cell attachment can be reached [22]. Porosity can also be a way to tune the stiffness of a material, as it happens for natural bones [23]. In this way, it is possible to reduce the stiffness of biomedical materials, to match that of natural bone tissue, thus limiting the so-called "stress shielding" effect [24].

The surface porosity fraction for FHA was estimated by potentiodynamic polarization using the following equation:

$$p = \frac{R_p}{R_p^0} \times 10^{-\left(\frac{\Delta E_{cor}}{\beta a}\right)} \tag{18}$$

Where R_p and R_p^0 are the polarization resistances of the bare substrate and the coating/substrate pair, respectively, $\Delta Ecorr$ is the potential difference between them, and βa is the anodic Tafel coefficient of the substrate.

The calculated values of the coating porosity from the potentiodynamic analyses are listed in Table 2.

The coating protective efficiency (Pi) can be calculated using the using the following equation [25]:

$$P_i = 100 \times \left(1 - \frac{R_p^0}{R_p}\right) \tag{19}$$

Where R_p^0 and R_p are the polarization resistances of the uncoated/ substrate coated bare substrate. The protective efficiency calculated for equation 19 is shown in Figure 7.

FHA coating showed a higher protective efficiency in physiological serum than in artificial saliva. It can be seen that the corrosion rate of CoCrMo improved, after FHA coating. FHA inhibits the corrosive action of the artificial saliva or physiological serum from penetrating into the substrate. FHA coating reduce the diffusion of the corrosive medium into the substrate and hence, decline the corrosion rate.

Table 2

Chemical composition of artificial saliva Afnor/ *Compoziția chimică saliva artificială Afnor*

Substance	NaCl	KCl	Na_2HPO_4	$NaHCO_3$	KSCN	CH_4ON_2
Quantity (g/L)	0.7	1.2	0.26	1.5	0.33	1.3

Table 3

Electrochemical parammetres from Tafel plots/ *Parametri electrochimici din curbele Tafel*

Solutions	Artificial saliva (Afnor)		Physiological serum (NaCl 0.9%)	
Electrodes	CoCrMo	CoCrMo/FHA	CoCrMo	CoCrMo/FHA
$i_{corr}[\mu A/cm^2]$	0.258	0.099	0.546	0.125
Ecorr [V]	-0.481	0.055	-0.381	0.111
$R_p [\Omega/cm^2]$	$10.63 \cdot 10^4$	$21.72 \cdot 10^4$	$33.58 \cdot 10^3$	$11.42 \cdot 10^4$
Vcorr [mm/Y]	$2.96 \cdot 10^{-3}$	$1.139 \cdot 10^{-3}$	$5.46 \cdot 10^{-3}$	$1.72 \cdot 10^{-3}$
P(%)	-	13.41	-	14.64
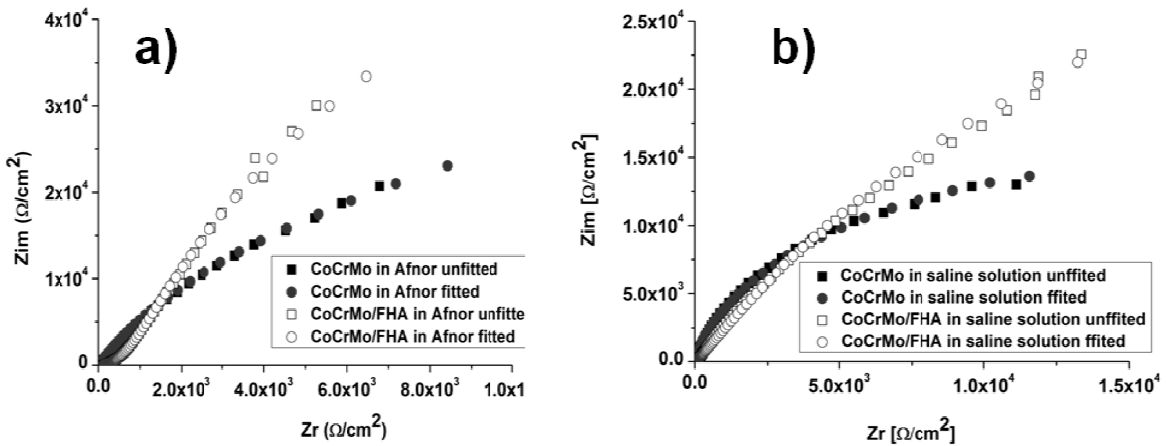
Fig. 8 - Nyquist diagrams for CoCrMo and coated CoCrMo in artificial saliva and in saline solution/ *Diagramele Nyquist pentru CoCrMo acoperit și neacoperit în soluție de salivă artificial și soluție salină*

.
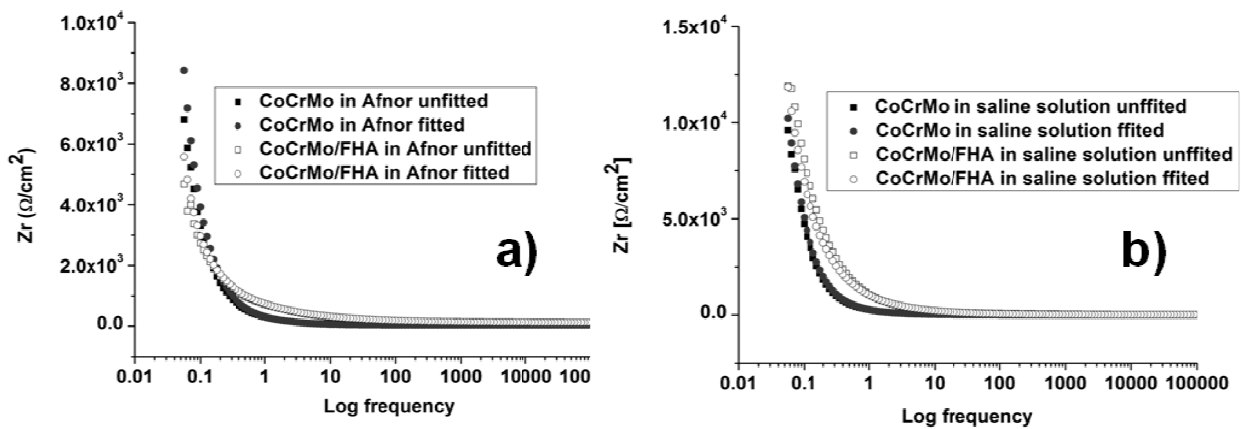
Fig. 9 - Bode diagrams for CoCrMo and coated CoCrMo in artificial saliva and in saline solution/ *Diagramele Bode pentru CoCrMo acoperit și neacoperit în soluție de salivă artificial și soluție salină.*
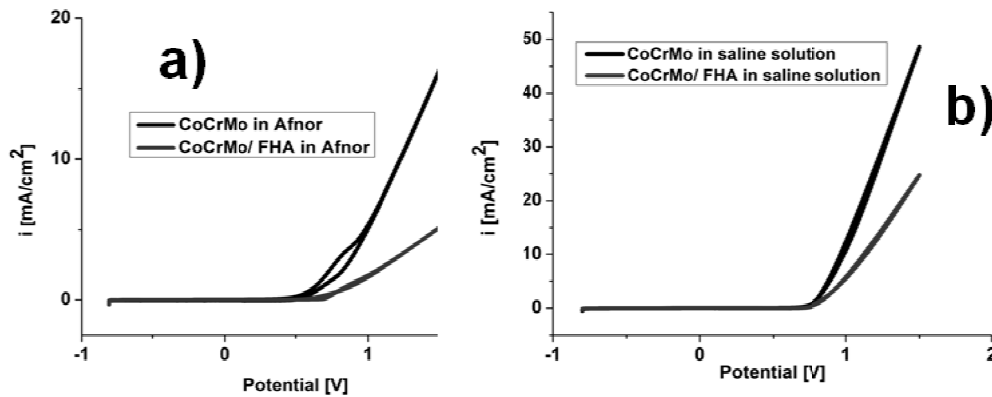
Fig. 10 - Cylic Voltammetry plots for coated and uncoated CoCrMo samples/ *Curbele de volatametrie ciclică pentru probele de CoCrMo acoperite şi neacoperite*

Electrochemical Impedance Spectroscopy

The Electrochemical Impedance Spectroscopy (EIS) determinations were performed using working parameters for initial frequency 100 KHz, final frequency 50 MHz and 10mV amplitude. The three electrodes system was the same: Ag/AgCl, Pt, CoCrMo and CoCrMo coated.

Figure 8 present Nyquist diagrams for coated and uncoated CoCrMo in artificial saliva and in saline solution.

Figure 9 present Bode diagrams for coated and uncoated CoCrMo in artificial saliva and in saline solution.

Electrochemical parameters from electrochemical impedance spectroscopy determinations are presented in Table 4, where Rsol (R1) is solution resistance, Rp (R2) is load transfer resistance (polarisation resistance at CoCrMo/ electrolyte interface), CPE1 is constant phase element (electric double layer capacitance at the interface CoCrMo/ electrolyte) and CPE2 is constant phase element of the coating/ electrolyte interface.

The EIS results indicated that the CoCrMo surface is composed of a bi-layered oxide consisting of an inner barrier layer associated to high impedance and responsible for corrosion protection, and an outer porous layer of lower impedance, which can sustain a suitable behaviour in bioapplication, including cell adhesion.
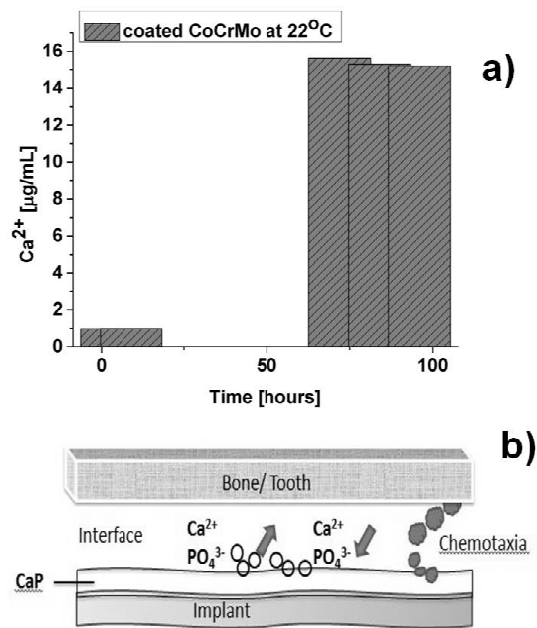
Fig. 11 - a) Ca^{2+} release in NaCl 0.9%/ *Dizolvarea ionilor Ca^{2+} in NaCl 0.9%;* b) An empirical model of calcium ions dissolution at interface/ *Un model empiric al dizolvării ionilor de calciu la interfață.*

Table 4

Electrochemical paramettres from EIS diagrams/ *Parametri electrochimici din diagramele EIS*

Solutions/ *Soluții*	Artificial saliva/ *Saliva articifială*		Saline Solution/ *Soluție salină*	
Electrodes	CoCrMo	**CoCrMo/FHA**	CoCrMo	**CoCrMo/FHA**
Electric circuit				
Rsol (R1) [Ω/cm^2]	29.70	119.31	9.58	15.31
Rp (R2) [Ω/cm^2]	$11.54\cdot10^4$	$27.52\cdot10^4$	$32.907\cdot10^3$	$10.29\cdot10^4$
CPE_1	$0.10\cdot10^{-3}$	$10.03\cdot10^{-5}$	$12.40\cdot10^{-5}$	$9.73\cdot10^{-5}$
n_1	0.91	0.99	0.91	0.81
CPE_2	-	$50.34\cdot10^{-5}$	-	$93.25\cdot10^{-5}$
n_2	-	0.48	-	0.49

In both cases, in physiological serum and in artificial saliva, the coating layer improves the resistance of the substrate (Rp values). Also Rp values are correlated with values obtained from Tafel plots. In artificial saliva, both studied materials covered and uncovered, shows a better corrosion resistance compared to physiological serum. Can be noticed that in case of CoCrMo/ physiological serum the Rp value is with an order of magnitude smaller than the CoCrMo/ artificial saliva, indicating a much more aggressive character of the serum. From the values of n1 and n2 we can say that at the interface of the CoCrMo/ electrolyte exist a capacitive character and at the interface of CoCrMo/FHA/electrolyte we have a diffusive character through obtained porous layer.

Cyclic Voltammetry

For cyclic voltammetry determinations the working parametters were: E_0 = -800mV, E_1 = -800mV, E_2 = 1500 mV and scan rate 2mV/seconds. In Figure 10 are shown cyclic voltammetry curves for uncoated and coated CoCrMo samples in solutions, artificial saliva and physiological serum.

All electrochemical characterizations confirm that the phosphate masses coating has improved corrosion resistance. Regarding the aggression of the solutions studied the results led to the fact that that saline solution has a more aggressive character due to free Cl^- ions in solution, which causes a stronger corrosion.

3.3.2. Ca^{2+} ion release in saline solution (NaCl 0.9%)

Calcium ions release on coated CoCrMo sample obtained at 22^0C in saline solution is presented in Figure 11 together with an empirical model of dissolution at interface. The observation time was until 100 hours and it is to mention that the evolution in time represents a trend to steady state.
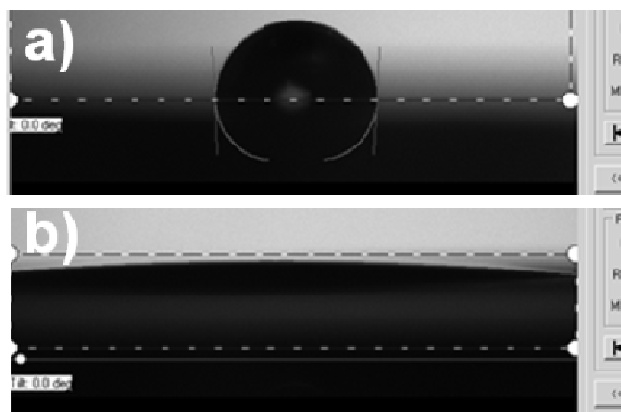
Fig. 12 - Contact angle values for uncoated (a) and coated CoCrMo sample (b)/ Valorile unghiului de contact pentru proba CoCrMo neacoperită (a) şi acoperită (b).

3.4. Contact Angle measurements

The determination of contact angle was performed with CAM 100 Equipment. The procedure supposes to place an equal volume (drop) of distilled water on samples surface.In Figure 12 the values represent the average from 5 determinations.

For all uncoated CoCrMo the contact angle values are bigger than 95^0 and the average is 96.3^0 which indicate a hydrofob character.

In case of CoCrMo with fluoridated phosphate masses coating the average for contact angle is 15.3 fact that puts in evidence the superhydrophilic character. The hydrophilicity is in relation with biocompatibility and for small contact angles the biocompatibility is higher.

3.5. Microhardness and Adherence tests

The Vickers test used for Microhardness determinations of metallic materials was performed with Buehler equipment by applying a load of 200 g for 10 seconds and was expressed by using the Vickers units (µHV).

The obtained value for coated CoCrMo alloy was 469 HV. Comparing with the standard value 310 HV according to ASTM F75, the obtained value is higher and indicates better hardness due to the coating layer.

Adhesion of studied coatings was determined according to ASTM D4511 with a device for determining the adhesion type PosiTest Pull- off adhesion AT-A (DeFelsko , USA).

Protective coating adhesion was evaluated by determining the highest pullout strength (pull-off Strength) which is required for detach a dolly attached with adhesive coating. This dolly (10mm diameter) was closely related to the sample's surface covered with epoxy resin adhesive in two components (epoxy-patch-907 Hysol Loctite / Henkel). The adhesive was allowed to strength for 72 hours at room temperature. Tests were made with the speed of 0.875 MPa.

By comparison the literature data of the adherence tests [26], the obtained values for coated CoCrMo samples are modest (2.79 MPa and 2.69 MPa), probably due to the fact that the coating layer was not uniform.

4. Conclusions

SEM and EDX analysis confirm that the electrochemical method for deposition of phosphate masses on CoCrMo is efficient. X-Ray Diffraction analysis proves the existence of mineralogical crystalline phases of fluorohydroxyapatite and $CaHPO_4$ as well.

An efficiency evaluation was quantified using electrochemical and mechanical measurements and we found that fluoridated phosphate masses electrodeposited on CoCrMo alloy is more stable in both electrolyte artificial saliva and physiological NaCl solution respectively.

The mechanical properties meaning microhardness and adherence are better for nanosized coatings as well.

REFERENCES

1. N. Maruyama, H. Kawasaki , A. Yamamoto , S. Hiromoto, H. Imai, and T. Hanawa, Friction-Wear properties of Nickel-Free Co-Cr-Mo alloy in a simulated body fluid, Materials Transactions, 2005, **46** (7), 1588.
2. G. Manivasagam, D. Dhinasekaran, and A. Rajamanickam, Biomedical Implants: Corrosion and its Prevention - A Review, Recent Patents on Corrosion Science, 2010, **2**, 40.
3. D. Ioniță, I. Man, and I. Demetrescu, The behaviour of electrochemical deposition of phosphate coating on CoCr bio alloys, Key Engineering Materials, 2007, **330-332**, 545.
4. Arnold H. Deutchman, Robert J. Partyka, and Robert J. Borel, Orthopaedic implants having self-lubricated articulating surfaces designed to reduce wear, corrosion, and ion leaching, US Patent No 20080221683, September, 11, 2008.
5. D. Portan, D. Ioniță, and I. Demetrescu, Monitoring TiO_2 nanotubes elaboration condition, a way for obtaining various characteristics of nanostructures, Key Engineering Materials, 2009, **415**, 9.
6. ASTM F75-12 Standard Specification for Cobalt- 28 Chromium-6 Molybdenum Alloy Castings and Casting Alloy for Surgical Implants (UNS R30075), doi:10.1520/F0075-12.
7. G. Totea, I.V. Branzoi, and D. Ioniță, Lactic acid influence on the electrochemical behaviour of stainless steel and CoCrMo alloy in human serum, Revista de Chimie, 2013, **64** (6) ,625.
8. M. Mindroiu , E. Cicek, F. Miculescu, and I. Demetrescu, The influence of thermal oxidation treatment on the electrochemical stability of TiAlV and TiAlFe alloys and their potential application as biomaterials, Revista de Chimie, 2007,**58** (9), 858.
9. P. Huang, and H.F. Lopez, Strain induced epsilon-martensite in a Co-Cr-Mo alloy: grain size effects, Materials Letters, 1999, **39** (4), 244.
10. I. Milošev, and H.-H. Strehblow, The composition of the surface passive film formed on CoCrMo alloy in simulated physiological solution, Electrochimica Acta, 2003, **48** (19), 2767.
11. IARC Monographs on the Evaluation of Carcinogenic Risks to Humans, Surgical Implants and other Foreign Bodies (International Agency for Research on Cancer, World Health Ornization, **74**, Lyon, France, 1999.
12. D. Ioniță, C. Ungureanu,and I. Demetrescu, Electrochemical and Antibacterial Performance of CoCrMo Alloy Coated with Hydroxyapatite or Silver Nanoparticles, Journal of Materials Engineering and Performance, 2013, **22** (11), 3584.
13. E.Dinu, M.Bîrsan,C.Ghițulică, G.Voicu, and E. Andronescu, Synthesis and characterization of hydroxyapatite obtained by sol – gel method, Romanian Journal of Materials, 2013, **43** (1), 55.
14. V. Stanic, Dj. Janackovic, S. Dimitrijevic, S. B. Tanaskovic, M. Mitric, M. S. Pavlovic, A. Krstic, D. Jovanovic, and S. Raicevic, Synthesis of antimicrobial monophase silver-doped hydroxyapatite nanopowders for bone tissue engineering, Applied Surface Science, 2011, **257** (9), 4510.
15. S. Overgaard, K. Soballe, K. Josephsen, E.S. Hansen, and C. Bunger, Role of different loading conditions on resorption of hydroxyapatite coating evaluated by histomorphometric and stereological methods, Journal of Orthopaedic Research, 1996, **14** (6), 888.
16. F.Bir, H. Khireddine, A. Touati, D. Sidane, S. Yala, and H. Oudadesse, Electrochemical depositions of fluorohydroxyapatite doped by Cu^{2+}, Zn^{2+}, Ag^+ on stainless steel substrates, Applied Surface Science, 2012, **258** (18), 7021.
17. J. Wang, Y. Chao, Q. Wan, Z. Zhu, and H. Yu, Fluoridated hydroxyapatite coatings on titanium obtained by electrochemical deposition, Acta Biomaterialia, 2009, **5** (5) ,1798.
18. G. Totea, D. Ioniță, R. M. Katunar, S. Cere, and I. Demetrescu Elaboration and characterization of the electrodeposited phosphates masses doped with various ions on stainless steel, Digest Journal of Nanomaterials and Biostructures, 2014, **9** (2), 575.
19. C. Wen, S. Guan, L. Peng, C. Ren, X. Wang, and Z. Hu, Characterization and degradation behavior of AZ31 alloy surface modified by bone-like hydroxyapatite for implant applications, Applied Surface Science, 2009, **255** (13-14), 6433.
20. N. Dumelie, H. Benhayoune, C. Rousse-Bertrand, S. Bouthors, A. Perchet, L. Wortham. J. Douglade, D. Laurent-Maquin, and G. Balossier, Characterization of electrodeposited calcium phosphate coatings by complementary scanning electron microscopy and scanning-transmission electron microscopy associated to X-ray microanalysis, Thin Solid Films, 2005, **492** (1-2), 131.
21. G. Pennel, G. Leroy, C. Rey, B. Sombret, J.P. Huvenne, and E. Bres, Infrared and Raman microspectrometry study of fluor-fluor-hydroxy and hydroxyl-apatite powders, Journal of Materials Science: Materials in Medicine, 1997, **8**, 271.
22. M. Rouahi, E. Champion, P. Hardouin, and K. Anselme. Quantitative kinetic analysis of gene expression during human osteoblastic adhesion on orthopaedic materials, Biomaterials, 2006, **27** (14), 2829.
23. M.B. Schaffler, and D.B. Burr, Stiffness of compact bone: Effects of porosity and density. Journal of Biomechanics, 1988, **21** (1), 13
24. K. S. Katti, Biomaterials in total joint replacement, Colloids and Surfaces B: Biointerfaces, 2004, **39** (3), 133.
25. H.-G. Kim, S.-H. Ahn, J.-G. Kim, S. J. Park, and K.-R. Lee, Corrosion performance of diamond-like carbon (DLC)-coated Ti alloy in the simulated body fluid environment, Diamond and Related. Materials, 2005, **14** (1), 35.
26. D-M. Liu, Q. Yang, and T. Troczynski, Sol-gel hydroxyapatite coatings on stainless steel, Biomaterials, 2002, **23** (3), 691.

****